Journal of Applied Fluid Mechanics, Vol. 18, No. 6, pp. 1563-1575, 2025.
Available online at www.jafmonline.net, ISSN 1735-3572, EISSN 1735-3645.
https://doi.org/10.47176/jafm.18.6.3153

Research on the Effect of Small Blade Arrangement on the Cavitation Performance of Centrifugal Pumps

W. G. Zhao†, Y. Liu and J. Zhang

College of Energy and Power Engineering, Lanzhou University of Technology, Lanzhou, 730050, China

†Corresponding Author Email: zhaowg@zju.edu.cn

ABSTRACT

This study proposes a novel approach to enhance the cavitation performance of centrifugal pumps with low specific speed by incorporating small blades within the impeller flow channel. These blades are deflected at specific angles at their trailing edges to suppress cavitation and improve pump efficiency. Experimental tests were conducted to assess the external characteristics and cavitation performance of a prototype pump, and the results were compared with numerical simulations. The findings indicate that the addition of small blades has minimal impact on the pump's external characteristics but significantly enhances its cavitation performance. Specifically, the low-pressure regions and areas of high-intensity turbulent kinetic energy within the impeller were reduced. Consequently, the volume of cavitation bubbles and the amplitude of pressure pulsation decreased. Flow field analysis revealed that the modified flow structure is more stable, with reduced vortex intensity. The small blades effectively align disordered turbulent flow lines, thereby suppressing cavitation development.

Article History

Received September 30, 2024
Revised January 21, 2025
Accepted February 3, 2025
Available online March 30, 2025

Keywords:

Centrifugal pump
Cavitation suppression
Small blade
Pressure pulsation
Flow field structure

1. INTRODUCTION

Pumps play a vital role in fluid transportation and are often referred to as the "heart" of modern industry. However, cavitation presents a major challenge to their performance. Unique to liquid media, cavitation is a phase change phenomenon that occurs in fluid equipment operating with liquid. In centrifugal pumps, cavitation is almost unavoidable, leading to disrupted water flow continuity and reduced efficiency in fluid machinery. In severe cases, it can damage the machinery's overflow surfaces, significantly impairing pump functionality and posing substantial operational challenges. This, in turn, hampers the development of the fluid machinery industry.

Zhu et al. (2024) explored the mechanisms of cavitation in centrifugal pumps and its associated hazards. Their research also reviewed the current state of cavitation monitoring methods, providing a comparative analysis of commonly used techniques. Enhancing the performance of low specific speed centrifugal pumps is particularly significant. Implementing effective measures to suppress cavitation is essential for the safe operation of hydraulic machinery. Additionally, a thorough understanding of cavitation mechanisms is critical. Such knowledge not only aids in mitigating cavitation but also contributes to improving the overall safety and efficiency of hydraulic systems.

Current analytical studies on cavitation often integrate experimental investigations with numerical simulations. Pang et al. (2024) introduced a J-groove design method. They found that the J-grooves on the pump cavitation, pressure fluctuations have obvious inhibition effect. However, the pump efficiency will be reduced. Kurokawa et al. (1999) applied J-grooves to a mixed-flow pump, finding that they improved the stability of the pump's characteristic curve by mitigating vortex-induced instabilities. This modification successfully controlled and suppressed rotational stall in the diffuser of centrifugal turbomachinery. Li et al. (2024) developed a periodic jet system inspired by fish gill respiration. They applied it to Clark-Y hydrofoils. Their results showed that the system maintained the hydrofoil's lift-to-drag ratio while significantly reducing cavitation, particularly under high-speed flow conditions. Gu et al. (2023) designed a bionic shark gill slit jet structure. They used numerical simulations to analyze its impact on the suction surface of hydrofoils under high-speed flow. The simulations revealed a significant reduction in the mean cavitation bubble volume fraction, offering valuable insights into hydrofoil performance in such conditions. Yun et al. (2023) proposed an active cavitation suppression

NOMENCLATURE

b_1	impeller outlet width	r_b	vacuole radius,
C_μ	viscosity coefficient	S_i	generalized source term
D	diameter of connection between blade inlet and front cover	t	time
D_1	impeller inlet diameter	u	mixture velocity
D_2	impeller outlet diameter	u_1	circular velocity
D_3	base circle diameter of volute	x	spatial coordinate
F_{cond}	condensation coefficient	Z	blade number
F_{vap}	vaporization coefficient	α_l	volume fraction of clear water medium;
f_v	vapor phase mass fraction	α_{nuc}	cavitation nucleus volume fraction
H_0	head	α_v	vapor volume fraction
i	different dimensions of the fluid movement in three-dimensional space, i,=1,2,3	β_1	inlet blade angle
j	different dimensions of the fluid movement in three-dimensional space, j=1,2,3	β_2	outlet blade angle
k	turbulence kinetic energy	η	efficiency
n_s	specific speed	μ	dynamic viscosity
p	pressure	μ_m	mixture dynamic viscosity
P_{in}	reference static pressure	μ_t	turbulent viscosity
p_v	saturated vapor pressure	ρ_l	liquid-phase density
Q_0	flow rate	ρ_m	mixture density
R_c	condensation source term	ρ_v	vapor density;
R_e	evaporation source term	ω	dissipation frequency

structure incorporating jet holes on hydrofoil surfaces. Simulations showed that these jet holes effectively regulate the cavitation flow field, playing a crucial role in controlling the flow. Specifically, the jet holes on the suction surface significantly suppressed cavitation development, and limited cavitation detachment to a certain extent. Wang et al. (2023) investigated a hydrofoil with a tip gap, introducing a bionic wavy tip design for vortex and cavitation suppression. Numerical analysis revealed that this design reduced cavitation volume by 44%, effectively inhibiting cavitation. Yan et al. (2022) proposed two strategies to suppress cavitation and improve the performance of axial piston pumps. One is increasing the radius of the distributing circle. Another is reducing rotational speed. Their findings demonstrated that both methods effectively suppressed cavitation within the plunger cavity while enhancing the actual flow rate. Dönmez et al. (2018) studied the influence of inlet blade angles on the cavitation performance of centrifugal pumps. They found that variations in hub and shroud blade angles significantly affect cavitation performance. Specifically, increasing the hub blade angle slightly degrades cavitation performance. However, increasing the shroud blade angle from 20°to 30°improves it. Wang et al. (2022) designed outlet blades with varying angles. Their results indicated that increasing the outlet blade angle gradually weakened pressure fluctuations at all monitoring points. The pressure fluctuations correlated with changes in the outlet blade angle. Wang et al. (2024b) explored cavitation suppression in low-speed centrifugal pumps. They introduced a biomimetic blade design inspired by the humpback whale. They employed the SST turbulence model to analyze the entire pump flow channel. Their study compared cavitation bubble volume fraction, static pressure distribution, turbulent kinetic energy, vortex volume, and streamline effects. The results provide theoretical insights for improving cavitation performance and operational stability in centrifugal pumps. Ma et al. (2024) compared the performance of equal-pitch and variable-pitch inducers. Experimental results showed that both inducers exhibit excellent anti-cavitation performance, effectively suppressing cavitation development. To improve the NPSH performance of water jet propellers, Wang et al. (2024a) designed a bionic impeller with a non-smooth leading edge. Simulations of the viscous flow field were conducted to analyze flow characteristics, including streamlines, pressure distribution, and vortex formation around the bionic blade. This optimization enhanced cavitation distribution and strength, thereby improving hydrodynamic performance. Dong et al. (2024) studied the impact of the number of guide blades on cavitation performance. They also analyzed the pressure fluctuations in the vaneless zone of the pump. The results indicate that changes in the number of guide blades affect the frequency of pressure peaks and valleys. This effect was observed at each monitoring point throughout the cycle. Additionally, increasing the number of guide blades reduces the amplitude of pressure fluctuations. It also reduces the pressure differentials. These changes contribute to a more stable operational state of the unit. Weiguo and Bao (2021) proposed placing obstacles on the suction and pressure surfaces of blades to suppress cavitation. Their findings demonstrated that these obstacles significantly reduced turbulent kinetic energy near the inner wall of the impeller channel. Additionally, the distribution of cavitation bubbles was decreased. This resulted in more stable flow within the impeller and effectively controlled cavitation progression. Zakir and Zhao (2024) developed a method to control cavitation flow instability in centrifugal pumps. They arranged obstacles on blade surfaces. Their findings revealed that the introduction of these obstacles significantly reduced the intensity of turbulent kinetic energy. This effect was observed near the inner wall of the

impeller channel. Additionally, they significantly decreased the growth rate of cavitation volume, enhancing flow stability. Qiu and Fang (2017) investigated the internal and external characteristics of low specific speed centrifugal pumps. Their study found that incorporating diverter blades enhanced both the pump head and efficiency. The diverter blades also suppressed flow separation on the pressure surface of the blades, effectively reducing flow losses. He et al. (2004) conducted a three-dimensional numerical simulation. The simulation focused on turbulence in the flow field of a diverter blade centrifugal pump impeller. Their results demonstrated a significant improvement in the "jet-wake" structure within the pump's internal flow field.

This paper focuses on low specific speed centrifugal pumps. It proposes a method of integrating small blades at the center of the pump impeller. These blades feature trailing edges deflected at specific angles. A combination of experimental testing and numerical simulations is used to evaluate the effects of these blades on cavitation performance. The study also analyzes the mechanisms of cavitation control, comparing results with and without the small blades.

2. PHYSICAL MODEL

2.1 Prototype and Modification

To study the effect of adding small blades to the impeller of centrifugal pump on the cavitation suppression, a low specific speed centrifugal pump was selected for the present research. The specified operating conditions are: rotational speed n=500 r/min and specific speed n_s=32. The pump model comprises six main components: inlet section, impeller, outlet section, front chamber, rear chamber, and volute. The key design parameters of the pump are as follows: flow Q_0=8.6 m^3 /h, design head H_0=4.2 m, impeller outlet diameter D_2=310 mm, impeller inlet diameter D_1=90 mm, impeller outlet width b_1=12 mm, the number of blades Z = 6, inlet blade angle and outlet blade angle β_1=β_2=37 °, base circle diameter of volute D_3=320mm, as shown in Fig. 1.

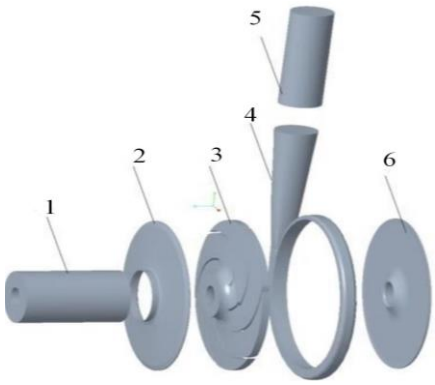

1.inlet section 2. front chamber 3.impeller 4.volute 5.outlet section 6.rear chamber

Fig. 1 Calculation field of the prototype pump

The centrifugal pump is modified by incorporating small blades into the impeller channel. The impeller design, shown in Fig. 2. It includes two configurations: one without small blades and another with small blades positioned in the center of the flow channel. The added blades are designed based on the prototype blade profile. Their thickness and height matching the original impeller blades. This design prevents flow field non-uniformity or flow separation caused by geometric differences, maintaining the pump's overall flow stability and efficiency. The small blades are 30 mm in length. According to the literature (Weiguo & Zhongliang, 2022), placing small blades near the impeller inlet enhances cavitation suppression. The impeller inlet is a region within the centrifugal pump where the pressure is relatively low and cavitation is likely to occur. The placement of small blades in this region can alter the fluid flow pattern entering the impeller, promoting a more orderly flow. Therefore, the small blades will be arranged 75mm away from the inlet. The trailing edge of each small blade is deflected by 12° towards the back of the blades. The blades are staggered and evenly distributed. The number of small blades matching that of the original impeller blades. These small blades are arranged circumferentially around the impeller.

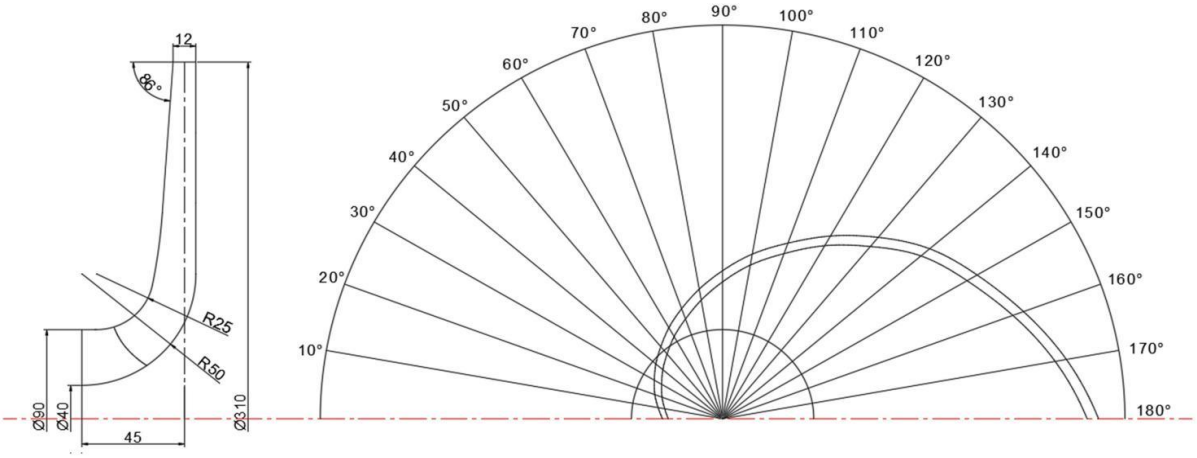

Fig. 2(a) Two-dimensional diagram of prototype impeller

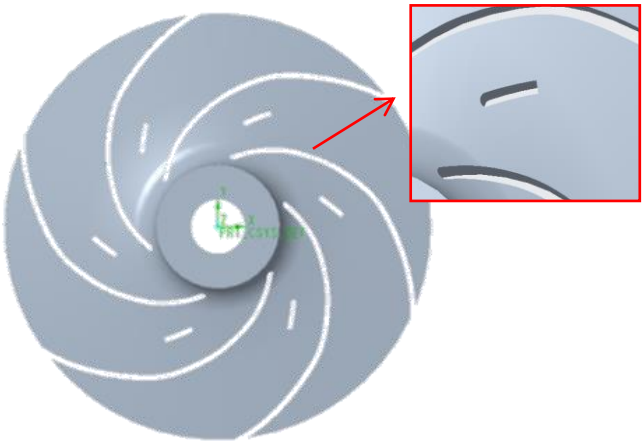

Fig. 2(b) Three-dimensional model of modified impeller

Table 1 Verification of grid-independence

Scheme	Number of impeller grids/10^6	Total number of grids/10^6	Experimental head	Head/m	η	Error/%
1	0.825	1.93	4.35	4.265	45	1.9
2	0.912	2.03	4.35	4.292	46	1.3
3	0.973	2.14	4.35	4.296	46	1.2
4	1.28	2.40	4.35	4.299	47	1.1

Fig. 3(a) Computational domain meshing for the centrifugal pump

2.2 Mesh Generation

The computational domain was meshed using ICEM 19.2. The centrifugal pump model was discretized using a hexahedral structured grid. To enhance accuracy, the near-wall region was refined during the meshing process to better capture the boundary layer flow. The meshing of the centrifugal pump's computational domain is shown in Fig. 3(a).

The principle of grid independence verification is to gradually encrypt the grid and observe the change trend of the simulation results. When the change of the results tends to be stable or fluctuating within an acceptable range, the grid is considered to be independent. To minimize errors caused by grid density variations, a mesh independence check and sensitivity analysis were performed. These variations can affect the simulation accuracy and reliability of the results. The original centrifugal pump model was divided into four grid density groups. As shown in Table 1, the head increases with the total number of grids, and efficiency follows a similar trend. It is found that the relative errors of head and efficiency with the change of mesh density are controlled within 3%, which indicates that the influence of the total number of elements on the numerical simulation can be negligible. The numerical simulation results of pump head under different mesh densities are compared with the experimental values, the error for Scheme 4 was controlled to approximately 1%. To optimize the computing resources, Scheme 4 was selected as the final grid configuration for the computational domain analysis.

When performing grid independence verification, it is necessary to ensure that the value of Y+ in the near-wall region satisfies the mesh quality requirements for the selected turbulence model. This ensure the practical significance of the grid independence results. The dimensionless Y+ value refers to the minimum vertical distance from the first grid cell node in the near-wall region to the wall. The turbulence model chosen in this study is the SST k-ω model, which requires the Y+ value in the boundary layer to be less than 100 (Jun, 2012). As shown in the Fig. 3(b), the Y+ values on the blade surface meet the requirements of this turbulence model.

Fig. 3(b). Y+ value distribution of impeller blade

3. NUMERICAL SIMULATION

3.1 Governing Equations

The fluid motion is governed by the Reynolds-averaged Navier-Stokes equations (Ferziger et al., 1997).

Continuity equation

$$\frac{\partial \rho_m}{\partial t}+\nabla\cdot(\rho_m u)=0 \tag{1}$$

Conservation of momentum equation

$$\frac{\partial(\rho u_i)}{\partial t}+\frac{\partial(\rho u_i u_j)}{\partial x_j}=-\frac{\partial p}{\partial x_i}+\frac{\partial}{\partial x_j}$$
$$[\mu(\frac{\partial u_i}{\partial x_j}+\frac{\partial u_j}{\partial x_i})]+Si \tag{2}$$

Transport equation

$$\frac{\partial(\rho_l \alpha_{l)}}{\partial t}+\frac{\partial(\rho_l \alpha_l u_j)}{\partial x_j}=R_e-R_c$$
$$\rho_m=\rho_l\alpha_l+\rho_v\alpha_v$$
$$\mu_m=\mu_l\alpha_l+\mu_v\alpha_v \tag{3}$$

where ρ_m is the mixture density, kg/m^3; ρ_l is the liquid-phase density; u is the mixture velocity, m/s; x is the spatial coordinate; subscripts i and j are between 1-3; t is time, s; p is pressure, Pa; μ_m is the mixture dynamic viscosity, N·s/m^2; μ is the dynamic viscosity R_e is the evaporation source term; and R_c is the condensation source term; α_v is the vapor volume fraction; α_l is the volume fraction of clear water medium; S_i is generalized source term.

3.2 Turbulence Model

Turbulence model is a mathematical model used to describe and simulate turbulent flow behavior. At present, RANS simulation is widely used in the engineering field because of its high computational speed. Reynolds Averaged Navier-Stokes Equation is an extension of momentum conservation equation in turbulent flow. It retains the essence of momentum conservation, but takes into account the additional effect of turbulence pulsation. The following will be an introduction to the Reynolds-Averaged Navier-Stokes (RANS) Method, this is used to average the time of turbulence to solve turbulence problems. Its expression is:

$$\frac{\partial(\rho_m u_i)}{\partial t}+\frac{\partial(\rho_m u_i u_j)}{\partial x_j}=-\frac{\partial p}{\partial x_i}+\frac{\partial}{\partial x_j}\left(\mu_m\frac{\partial u_i}{\partial x_j}-\rho_m\overline{u_i'u_j'}\right) \tag{4}$$

Where: $-\rho_m\overline{u_i'u_j'}$ is Reynolds stress.

Because of the Reynolds stress term included in the equation, the analytical solution cannot be obtained directly from the mean equation. Therefore, in order to make the equations closed, so that the turbulent Reynolds stress can be solved, a turbulence model based on the Reynolds Averaged Navier-Stokes Equation needs to be introduced. The specific form and number of equations that need to be added depend on the turbulence model used. The turbulence model selected in this study is the modified SST k-ω model. This model effectively predicts flow near the wall while performing well in other flow regions. This model combines the benefits of the k-ϵ model near the wall and the k-ω model in the free-stream region. This model also takes into account turbulent shear stress transport, so flow separation under various pressure gradients can be predicted. The SST k-ω model provides a more accurate representation of flow states and is considered more objective (Wilcox 1994; Wilcox 2008). In the cavitation zone of the centrifugal pump impeller, a gas-liquid two-phase mixture exists, with significant density differences. These density variations impact turbulent viscosity. To mitigate this effect, the density function $f(\rho m)$ is corrected as follows:

$$\mu_t=f(\rho_m)C_\mu\frac{k}{\omega} \tag{5}$$

$$f(\rho_m)=\rho_v+(1-\alpha_v)^n(\rho_l-\rho_v) \tag{6}$$

where α_v is the vapor-phase volume fraction; μ_t is the turbulent viscosity; ρ_m is the vapor-liquid mixed-phase density; ρ_l is the liquid-phase density; ρ_v is the vapor density; C_μ is the viscosity coefficient; k is the turbulence kinetic energy; ω is the dissipation frequency and n is a constant. By analyzing the effects of different values of n on the numerical calculation results for three-dimensional cavitation flow (Coutier-Delgosha et al., 2003), n=10 is taken in this paper for calculation.

3.3 Cavitation Model

The selection of an appropriate cavitation model is critical for accurate numerical simulation. In this study, the Zwart-Gerber-Belamri cavitation model (Zwart et al., 2004) is used. This model is widely recognized for its ability to accurately represent the gas-liquid phase transition. Additionally, it can correctly describe the series of changes in the cavitation bubbles. It is an improvement of the Kubota model, ignoring the second-order time derivative term and surface tension. It is able to better capture the specific details of the cavitation flow. It is widely used as the default cavitation model in CFX software. The model equations are as follows:

$$\frac{\partial(\rho_m f_v)}{\partial t}+\frac{\partial(\rho_m u_t f_v)}{\partial x_i}=R_e-R_c \tag{7}$$

$$R_e=F_{vap}\frac{3\alpha_{nuc}(1-\alpha_v)\rho_v}{r_b}\sqrt{\frac{2}{3}\frac{p_v-p}{\rho_l}}$$
$$(p\le p_v) \tag{8}$$

$$R_c=F_{comd}\frac{3\alpha_v\rho_v}{r_b}\sqrt{\frac{2}{3}\frac{p-p_v}{\rho_l}}$$
$$(p>p_v) \tag{9}$$

where f_v is the vapor phase mass fraction, p_v is the saturated vapor pressure, p_v=3169 Pa at 25°C; R_e is the evaporation source term; R_c is the condensation source term; ρ_l is the liquid-phase density; ρ_m is the mixture density, kg/m^3; F_{vap} is the vaporization coefficient, set to 50; F_{cond} is the condensation coefficient, set to 0.01; r_b is

the vacuole radius, set to 1×10^{-6} m; α_{nuc} is the cavitation nucleus volume fraction, set to 5×10^{-4}.

3.4 Boundary Conditions

Numerical simulations were conducted using ANSYS CFX 19.2 software. The boundary conditions for the computational domain were set as follows (Wang et al., 2022; Weiguo & Zhongliang, 2022): the impeller was modeled as a rotating domain. The surrounding regions were treated as stationary. A graphical representation of the boundary conditions is shown in Fig. 1, where the inlet (1) and outlet (5) sections are identified. The inlet was specified as a pressure inlet, and the outlet as a mass flow outlet. A pressure inlet was specified as the inlet boundary condition. A mass flow outlet was defined as the outlet boundary condition. The inlet pressure was adjusted to simulate varying degrees of cavitation development. Solid walls were treated as adiabatic, no-slip surfaces.

For the simulation, results from stationary calculations were used as initial values for the transient simulations. The freezing rotor model was selected for the dynamic-static interface in the stationary calculation. The transient freezing rotor model was used for the non-stationary calculation.

The fluid medium in the simulations was water at 25°C, with a constant time step of 1000 steps. Each time step had a rotational increment of 3°, consisting of 20 iterations with an iteration error threshold of 10^{-5}. After completing five calculation cycles, the internal fluid conditions were considered stable. Results from the final cycle were analyzed. The accuracy and stability of the centrifugal pump's numerical simulation process were ensured through this setup. This setting can contribute to a more accurate representation of the pump's flow characteristics and performance.

4. Experiment and Simulation

4.1 Experimental Device

The experiments focused on two main aspects: hydraulic performance and cavitation performance. These tests were conducted using a visualized closed centrifugal pump test bench at the Key Laboratory of Fluid Machinery and Systems in Gansu Province. The centrifugal pump was represented by a model. Clear water at room temperature was used as the test medium. This setup allowed for real-time observation of flow behavior and cavitation development.

The test bench is equipped with a stepless variable-speed motor for power control. Measurement instruments include speed sensors, pressure sensors, electromagnetic flowmeters, torque sensors, and vacuum sensors. Additional equipment includes a Φ1200×2600 cavitation tank, a liquid ring vacuum pump, and pipeline switch regulating valves. The structure of the test bench is shown in Fig. 4.

4.2 Algorithm Validation

The hydraulic performance of the centrifugal pump was tested to establish the relationship between pump

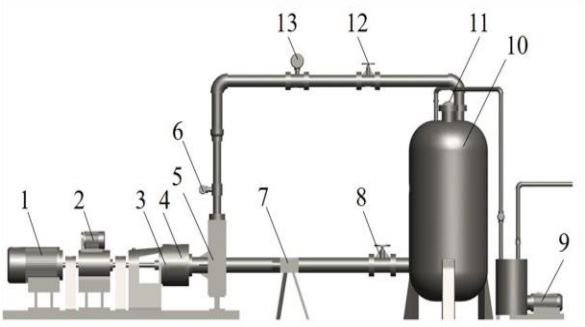

1.Motor; 2. Rotational speed and torque meter; 3.Stabilized flow tank; 4.Inlet pressure gauge; 5.Centrifugal pump visualization model; 6.Export pressure gauge; 7.High-speed camera; 8.Inlet regulating valve; 9.Liquid-ring vacuum pump; 10.Cavitation tank; 11.Vacuum gauge; 12.Export regulating valve; 13.Electromagnetic flowmeter.

Fig. 4 Closed test system of centrifugal pump

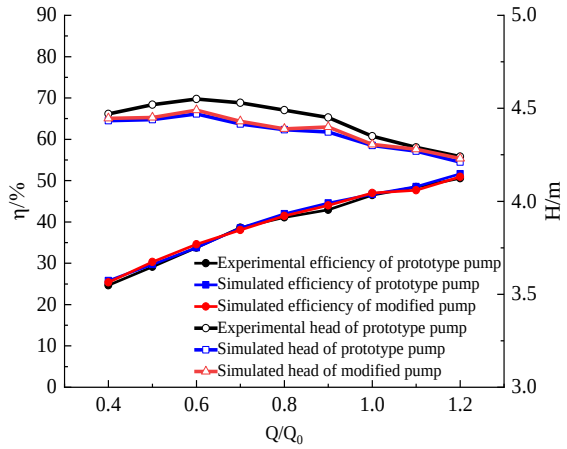

Fig. 5 External characteristic curves obtained from experiment and simulation

head, efficiency, and power by varying the pump's outlet flow rate. The tests were conducted across nine different operating conditions. Flow rates ranging from 0.4 to 1.2 times the design flow rate. Figure 5 shows a comparison of simulated values for the modified pump with small blades, alongside the experimental and simulation results for the prototype pump under various flow conditions. Under the design conditions, the simulated results for both the prototype pump and the modified pump are similar. The head and efficiency curves indicate that the maximum relative error in head is less than 1%, and the maximum relative error in efficiency is 2.5%. These findings suggest that the addition of small blades has minimal impact on the external characteristics of the pump.

In hydraulic machinery, the dimensionless cavitation number σ represents the likelihood and severity of cavitation:

$$\sigma = \frac{p_{in} - p_v}{0.5\rho u_1^2}, \tag{10}$$

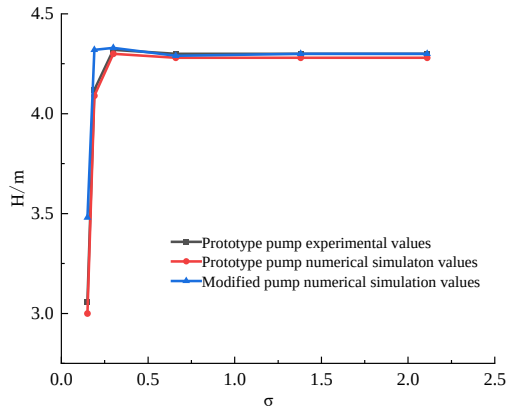

Fig. 6 Cavitation curves from experimental and simulation

where P_{in} is the reference static pressure (also the pump inlet pressure); P_v is the critical pressure, (the saturated steam pressure 3169 Pa); u_1 is the circular velocity at the junction between the blade inlet edge and the front cover plate. The velocity is given by $u_1 = n\pi D/60$, where D is the diameter of the junction between the blade inlet and the front cover plate.

In this test and simulation, the outlet flow rate of the centrifugal pump was kept constant. Cavitation was controlled by gradually reducing the inlet pressure. This allowed for the complete development of cavitation within the pump. Figure 6 presents the cavitation performance curves obtained from both experimental and simulation results.

As shown in Fig. 6, the cavitation performance curves for the prototype pump are consistent across different σ. Both simulation and experimental results matching closely. The error is controlled within 3%, confirming the accuracy of the numerical simulations.

The cavitation curves for both the prototype and modified pumps are shown. When σ is 0.19, cavitation causes the prototype pump's simulation head to break down. However, the small blade arrangement in the modified pump does not yet lead to head breakdown.

This arrangement effectively suppresses the formation of cavitation bubbles and delays cavitation onset in the centrifugal pump. Compared to the prototype, the modified pump increases the cavitation breakdown head by 14%. This demonstrates the effectiveness of the small blades in delaying cavitation. The following three graphs in Fig. 7 display the isosurface distribution of cavitation bubbles volume fraction (α_v = 10%) within the impeller at different σ values. The blue line represents the cavitation bubble morphology. The simulated cavitation bubble distribution with different σ values is basically consistent with the corresponding experimental results, as shown in Fig. 7. This confirms the reliability of the developed numerical algorithm.

5. RESULTS AND DISCUSSION

5.1 Variations in Bubble Volume

The volume of cavitation bubble inside the impeller is defined as:

$$V_{\text{cav}} = \sum_{i=1}^{N} \alpha_{v,i} V_i, \tag{11}$$

where N is the total number of control units in the computational domain; $\alpha_{v,i}$ is the vapor volume fraction in control unit i; and V_i is the control unit i volume.

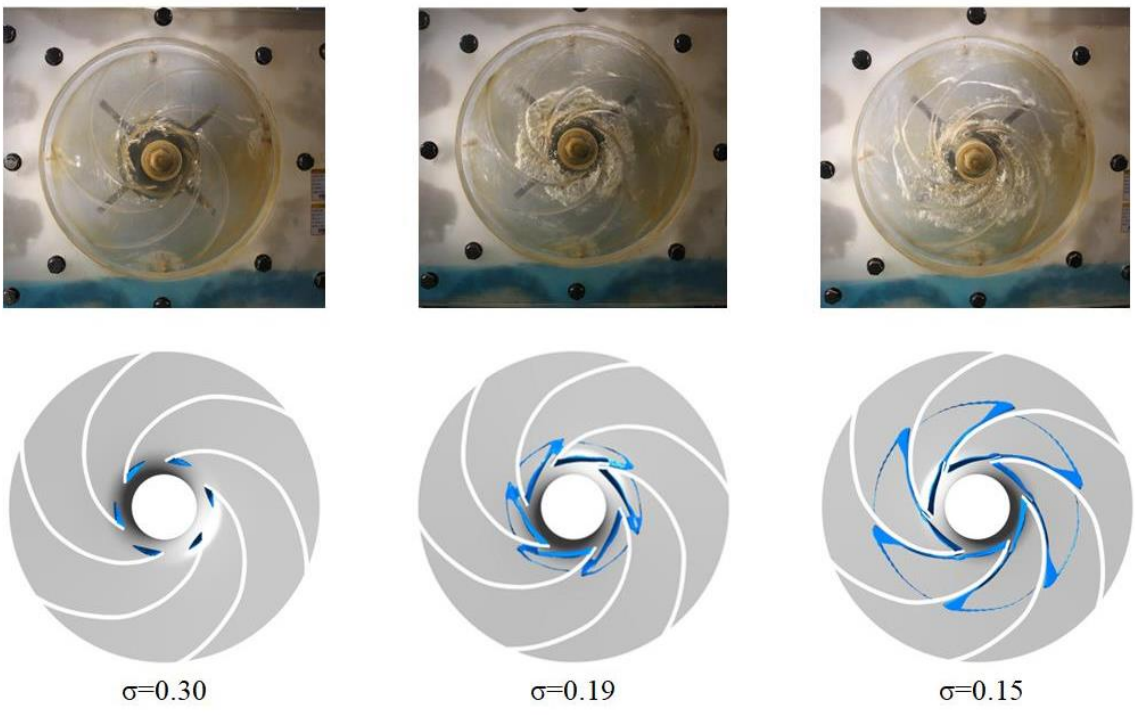

Fig. 7 Distribution of cavitation bubbles in the impeller(α_v=10%)

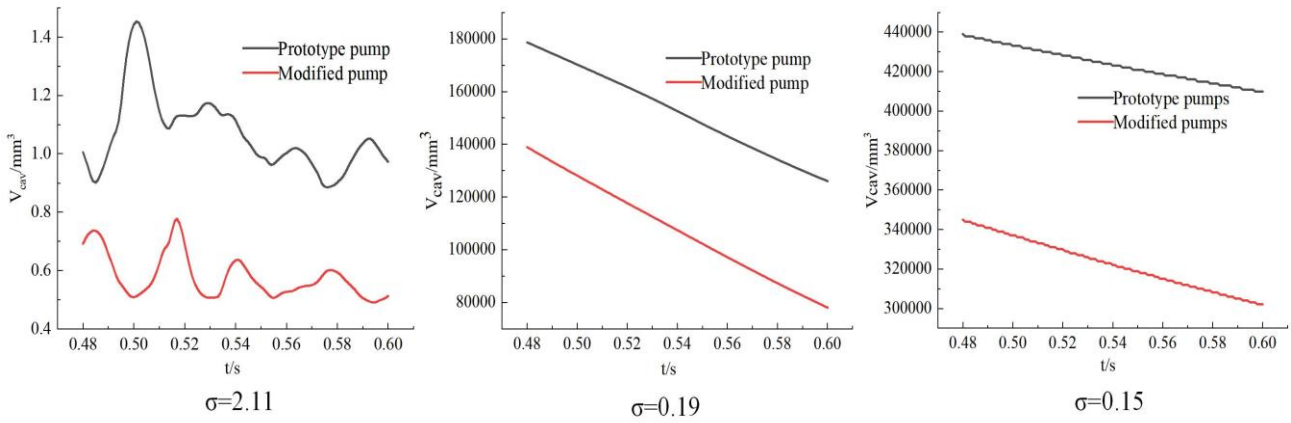

Fig. 8 Plot of volume fraction over time during the last cycle

Table 2 Average bubble volume values

	σ=2.11	σ=0.19	σ=0.15
average bubble volume of prototype pump/mm^3	1.067	152366	423677
average bubble volume of modified pump/mm^3	0.578	107690	322570
percentage reduction/%	45.9	30	24

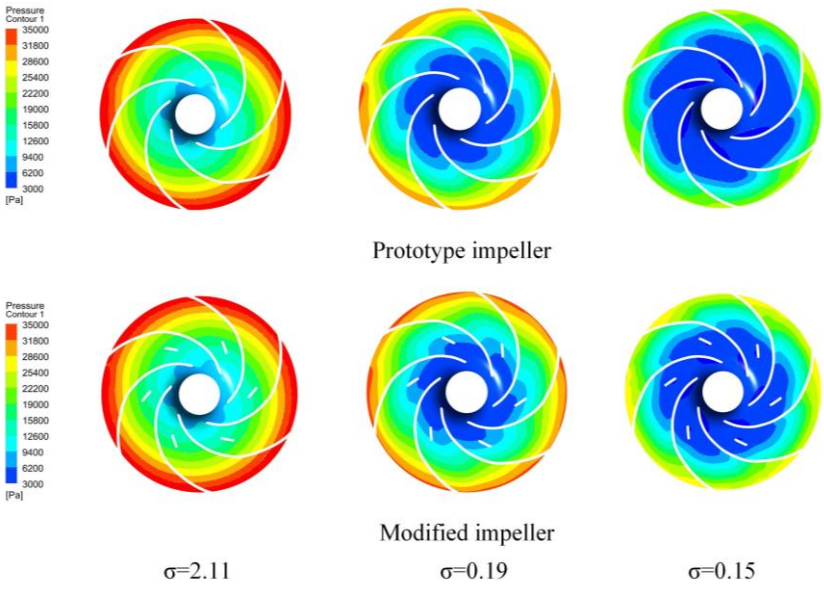

Fig. 9 Pressure distribution in the intermediate section

Figure 8 illustrates the variation in bubble volume over one rotation cycle of the impeller for different σ values. As cavitation progresses, the bubble volume within the impeller increases. Table 2 presents the average bubble volume values for both the prototype and modified pumps under different σ values. In the initial stage of cavitation, the modified pump shows a significant reduction in bubble volume—approximately 45.9% less than the prototype pump. As σ reaches 0.19, which is close to the critical cavitation point. The bubble volume in the modified impeller is reduced by about 30%. During the severe cavitation stage, the bubble volume in the modified pump is approximately 24% lower than that of the prototype pump. The small blades alter the local flow conditions, preventing the formation of low-pressure regions. They also induce relatively higher pressure within the impeller. This higher pressure reduces the appearance of cavitation. It also reduces the accumulation of cavitation bubble. These reductions lead to a decrease in overall bubble volume. Cavitation is inhibited by controlling the growth of cavitation bubble.

5.2 Variations in Pressure Distribution

Figure 9 illustrates the pressure distribution in the middle section of both impellers under different σ.

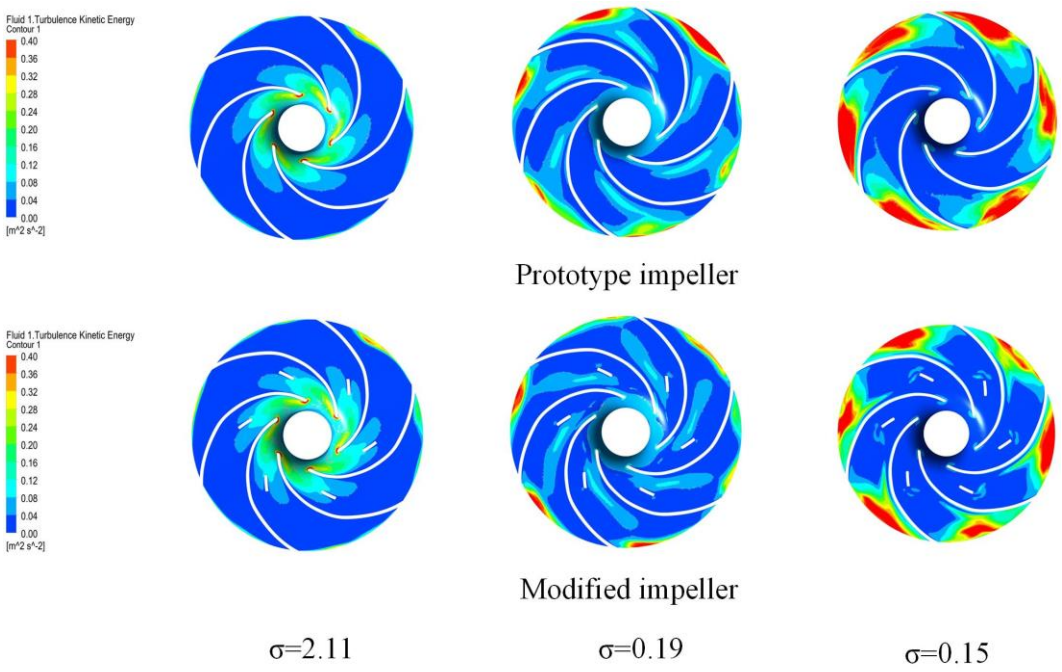

Fig. 10 Turbulent kinetic energy distribution in the intermediate section

As shown, the impeller inlet is a low-pressure region, which is where cavitation initially occurs. The absolute pressure increases radially along the impeller. As σ decreases, the low-pressure region within the impeller shifts toward the outlet and expands. A comparative analysis of the modified and prototype impellers reveals that at σ = 2.11, cavitation is minimal, with only a small low-pressure area at the impeller inlet. However, when σ drops to 0.19, significant differences emerge. The modified impeller effectively limits the expansion of the low-pressure region and reduces its size compared to the prototype impeller. When σ is 0.15, a severe cavitation stage occurs. With the addition of small blades, local high-speed flow is reduced by adjusting the flow direction. This inhibition of the velocity distribution prevents the sharp pressure drop caused by local high-speed flow. The overall pressure distribution becomes more uniform. In addition, the small blades mitigate low-pressure areas created by uneven flow by improving the flow field structure. They stabilize the fluid flow and reduce turbulence. Turbulence can cause energy dissipation and local pressure fluctuations, resulting in local low-pressure areas. The low-pressure region is the area where cavitation is easy to occur. Thus, cavitation is controlled by suppressing these low-pressure areas.

5.3 Variations in Turbulent Kinetic Energy Distribution

Turbulent kinetic energy is a critical parameter in turbulent flow, representing energy associated with turbulence. Elevated turbulent kinetic energy correlates with increased energy dissipation, resulting in higher flow losses in centrifugal pumps. Figure 10 depicts the turbulent kinetic energy distribution in both impellers for different σ values. High-intensity turbulent kinetic energy regions are predominantly located at the impeller inlet and the junctions with the volute.

At σ = 2.11, the high-intensity region is primarily concentrated at the impeller inlet. This concentration results from the fluid interacting with the blade's leading edge. This interaction creates complex turbulence structures, increasing turbulent kinetic energy. Compared to the prototype pump, the incorporation of small blades reduces the dispersion of turbulent kinetic energy, thereby decreasing the extent of high-turbulence regions. At σ = 0.19 and σ = 0.15, the areas of high turbulent kinetic energy diminish significantly. The small blades enhance flow stability and optimize the flow field structure. Preventing the formation of regions with high local velocity and pressure fluctuations. Consequently, the areas of elevated turbulent kinetic energy within the impeller flow channel are effectively minimized. Since high turbulent kinetic energy regions are often associated with low-pressure areas conducive to cavitation, reducing these regions mitigates cavitation occurrence. In addition, this reduction lowers energy dissipation and flow losses, improving overall pump performance.

5.4 Variations in Flow Field Structure and Cavitation Bubbles Morphology

Figure 11 illustrates the velocity vectors and cavitation bubble morphology for both impellers under different σ conditions. The figure reveals that most of the fluid exits the impeller channel along the suction surface, resulting in higher velocities near this surface. The velocity distribution at the impeller channel outlets remains generally consistent. However, downstream of the blade's trailing edge, flow line deflection occurs. This leads to a substantial increase in radial velocity on the pressure side of the impeller outlet blade. This results in the formation of a pronounced jet area. The interaction between the wake and the jet generates a significant velocity gradient. At σ = 2.11, the addition of small blades has minimal influence on the flow field distribution. As σ

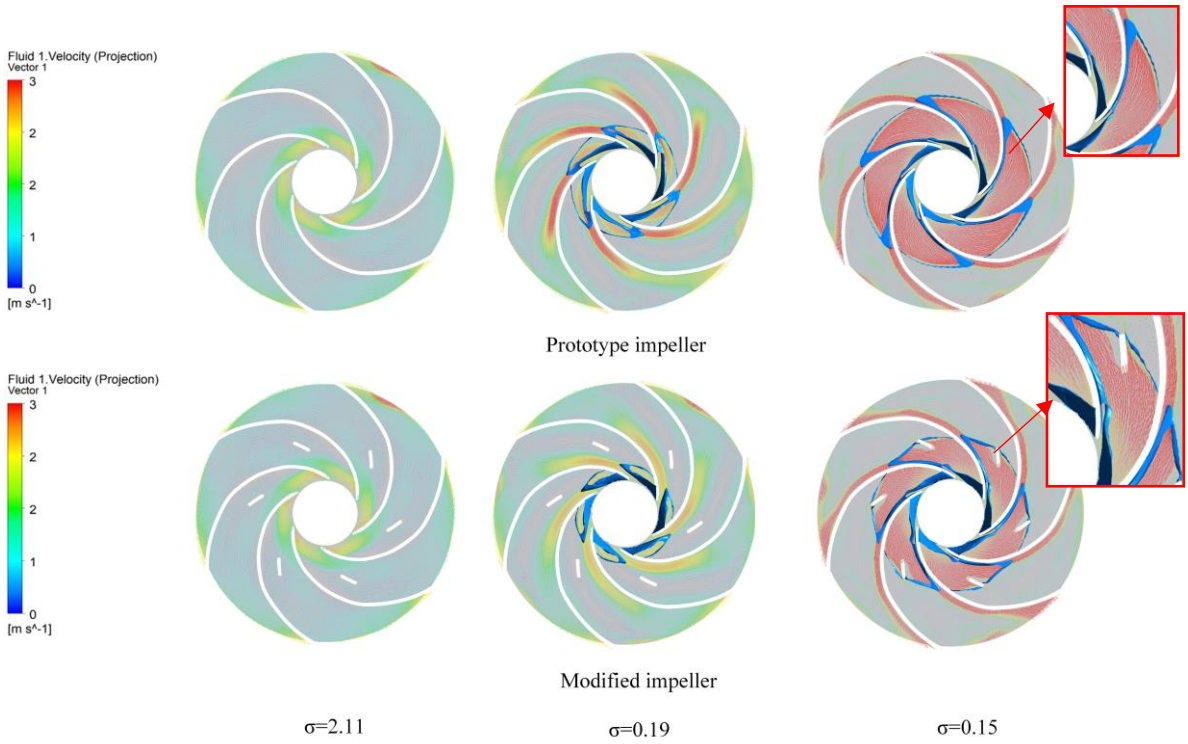

Fig. 11 Velocity vector diagram and bubbles morphology within the impeller

decreases, the flow within the impeller channel becomes increasingly turbulent. Vortex structures begin to form near the blade's trailing edge. These vortices propagate and expand at the impeller outlet, disrupting the flow within the channels. The figure demonstrates that the modified impeller breaks a large vortex region into two smaller regions. This alters the flow field structure and the flow pattern at the impeller inlet. This modification reduces the velocities of the jet and wake. The strength of the wake jet structure downstream of the blade's trailing edge is also diminished. The small blades also reduce flow separation on the blade surface, leading to a more uniform and optimized flow field distribution. Additionally, the small blades suppress vortex formation and perform flow rectification. These effects reduce energy losses and lead to a more stable flow field.

Figure 11 also depicts the isosurface distribution of the cavitation bubble volume fraction (α_v = 10%). This distribution is presented under different σ conditions. During the initial cavitation stage, the number and volume of cavitation bubbles are small. As a result, no distinct cavitation morphology is observed on either impellers. In the critical cavitation state and severe cavitation development stages, bubbles diffuse from the low-pressure region on the blade's back surface They then move along the flow path towards the working face. The cavitation region gradually expands and progresses towards the impeller outlet. Compared to the prototype impeller, the modified impeller exhibits a smaller cavitation area. The high pressure induced by the small blades suppresses cavitation development. This indicates that the addition of small blades effectively inhibits cavitation.

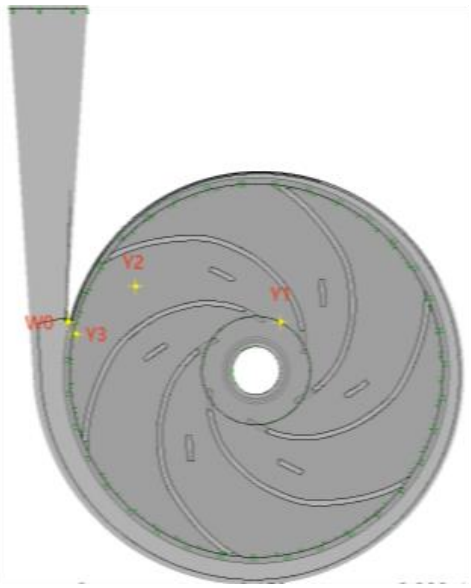

Fig. 12 Location of monitoring sites

5.5 Variations in Pressure Pulsation

Pressure pulsations significantly affect the performance of centrifugal pumps, contributing to noise and vibration. To analyze the impact of small blades on pressure pulsations, monitoring points were placed at key locations: the impeller inlet (Y1), inside the impeller flow channel (Y2), at the impeller outlet (Y3), and at the volute tongue (W0). The monitoring point locations are illustrated in Fig. 12.

The centrifugal pump analyzed operates at a rotational speed of 500 r/min with six blades (z = 6). The

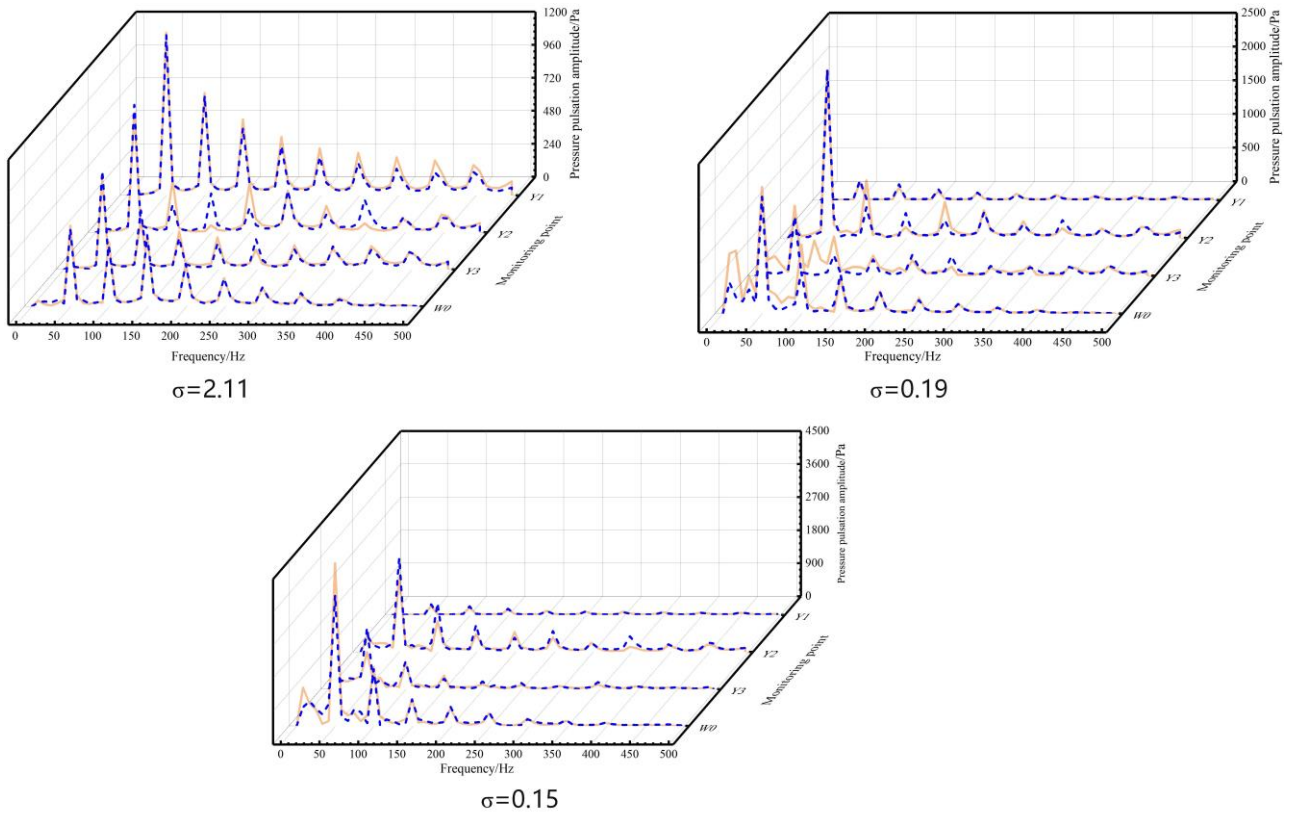

Fig. 13 Pressure pulsation spectrum at monitoring

calculated shaft frequency is 8.33 Hz, and the blade passing frequency is 50 Hz. Transient simulations were conducted for both the prototype and modified pumps, and time-domain pressure pulsation data were collected from the four monitoring points. A Fast Fourier Transform (FFT) was applied to these data, generating frequency-domain pressure pulsation spectra. Figure 13 displays the frequency-domain pressure pulsation graphs for both pumps under various cavitation conditions. The orange solid line represents the prototype pump, while the blue dashed line corresponds to the modified pump. The results show that the dominant frequency for both pumps at all monitoring points is 50 Hz. The amplitude decreases with increasing harmonics. This indicates that adding small blades does not alter the fundamental characteristics of pressure pulsation. Figure 13 illustrates the amplitude of the dominant pressure pulsation frequency at W0 across different σ values. For the modified pump, the amplitude is consistently lower than that of the prototype pump. The maximum reduction of 20%. The addition of small blades effectively streamlines the turbulent flow field. This reduction in turbulence lowers the pulsations caused by cavitation bubble shedding and collapse. During the early stages of cavitation, both the dominant and harmonic frequencies at Y1 in the modified pump are lower than those in the prototype pump. As cavitation advances to more severe stages, harmonic amplitudes at multiple monitoring points also decrease. The small blades optimize the flow field distribution, reducing pressure pulsations induced by turbulence. This optimization homogenizes the velocity distribution, minimizing pressure variations caused by velocity differences. It also reduces vortex strength, thereby preventing pressure fluctuations associated with vortices. These improvements contribute to suppressing cavitation development and alleviate noise and vibration resulting from cavitation.

6. CONCLUSION AND PROSPECT

This study examines the use of small blades to enhance the flow field structure and mitigate cavitation in centrifugal pumps. By incorporating small blades into the impeller flow channel, their impact on cavitation suppression is analyzed through experimental and numerical simulation results. The main conclusions are summarized as follows:

(1) Small blades with a 12° trailing-edge deflection were added into the impeller channel. The differences in external characteristics between the prototype and modified pumps were minimal, with the head-efficiency curves converging. However, the cavitation curve showed that the addition of small blades increased the pump's critical head, effectively delaying the onset of cavitation.

(2) The inclusion of small blades significantly reduces flow separation and organizes the turbulent flow field, leading to a more uniform flow distribution. This optimization minimizes flow losses and energy dissipation, reducing the high turbulent kinetic energy region. The high-pressure zone generated by the small blades suppresses bubble development, thereby inhibiting cavitation.

(3) The high pressure induced by the small blades significantly reduces cavitation bubble volume at various

cavitation stages. Additionally, the low-pressure zone within the impeller is minimized. The amplitude of pressure pulsation at some monitoring points is decreased. These effects effectively mitigate noise and vibration caused by cavitation.

There are several suggestions for future research.

(1) This study did not include hydraulic or cavitation performance tests for centrifugal pumps equipped with small blades. In future research, a plexiglass impeller with small blades can be fabricated. Then conduct comprehensive hydraulic and cavitation performance tests on the modified impeller.

(2) The current analysis focused exclusively on performance under the design flow condition. Future investigations should include both high-flow and low-flow conditions. This approach will enhance the applicability of the small-blade cavitation control method.

(3) Only one deflection angle was analyzed in this study. Future work should explore a wider range of control parameter and investigate the effects of multi-parameter coupling. This effort is essential to identify the optimal small-blade design for maximizing cavitation suppression performance.

ACKNOWLEDGEMENTS

This research was supported by National Natural Science Foundation of China (Grant No. 52169018) and the Central Government Guides Local Science and Technology Development Fund Projects（23ZYQA0320）

CONFLICT OF INTEREST.

The authors declare no conflicts of interest.

AUTHORS CONTRIBUTION

Weiguo Zhao: Conceptualization, funding acquisition, investigation, methodology, supervision, and visualization, and writing review & editing; **Ying Liu**: Conceptualization, data curation, methodology, formal analysis, validation, visualization., and writing-original draft; **Jing Zhang**: Conceptualization, data curation, formal analysis, methodology, validation, and visualization.

REFERENCES

Coutier-Delgosha, O., Fortes-Patella, R., & Reboud, J. L. (2003). Evaluation of the turbulence model influence on the numerical simulations of unsteady cavitation. *Journal of Fluids Engineering*, *125*(1), 38-45. https://doi.org/10.1115/1.1524584

Dong, W., He, F., Ai, G., Liang, W., Li, P., & Fan, X. (2024). *Effect of the number of guide vanes on cavitation characteristics and pressure pulsation of centrifugal pumps.* IOP Publishing Ltd. https://doi.org/10.1088/1742-6596/2707/1/012012

Dönmez, A. H., Yumurtacı, Z., & Kavurmacıoğlu, L. (2018). The effect of inlet blade angle variation on cavitation performance of a centrifugal pump: a parametric study. *Journal of Fluids Engineering*, *141*(2). https://doi.org/10.1115/1.4040557

Ferziger, J. H., Peric, M., & Leonard, A. (1997). Computational methods for fluid dynamics. *Physics Today*, *50*(3), 80-84. http://dx.doi.org/10.1007/978-3-319-99693-6

Gu, Y., Yin, Z., Yu, S. W., He, C., Wang, W., Zhang, J., Wu, D., Mou, J., & Ren, Y. (2023). Suppression of unsteady partial cavitation by a bionic jet. *International Journal of Multiphase Flow*. https://doi.org/10.1016/j.ijmultiphaseflow. 104466

Jun, Li, X., Yuan, S., Pan, Z., & Li, Y. (2012). Realization and application evaluation of near-wall mesh in centrifugal pumps. Nongye Gongcheng Xuebao/Transactions of the Chinese Society of Agricultural Engineering, 28(20), 67-72. https://doi.org/10.3969/j.issn.1002-6819.2012.20.009

Kurokawa, J., Saha, S. L., Matsui, J., & Kitahora, T. (1999). Passive control of rotating stall in a parallel-wall vaneless diffuser by radial grooves. *Journal of Fluids Engineering*, *122*(1), 90-96. https://doi.org/10.1115/1.483230

Li, J., Yan, H., & Wang, F. (2024). Suppression of hydrofoil unsteady cavitation by periodic jets based on fish gill respiration. *Ocean Engineering* (Feb.1), 293. https://doi.org/10.1016/j.oceaneng.2023.116584

Ma, L. L., Wang, C., Chen, Y., Wang, B. H., Yu, D. H., & Yang, Y. C. (2024). *The study of using the inducer to improve the cavitation performance of a centrifugal pump*. Journal of Physics: Conference Series, 2752(1). https://doi.org/10.1088/1742-6596/2752/1/012122

Pang, S., Zhu, B., Shen, Y., & Chen, Z. (2024). Study on suppression of cavitating vortex rope on pump-turbines by J-groove. *Applied Energy*, *360*. https://doi.org/10.1016/j.apenergy.2024.122843

Qiu, C., & Fang, X. (2017). Characteristics research of a low-specific-speed centrifugal pump with splitter blades. *Fluid Machinery*. https://doi.org/10.3969/j.issn.1005-0329.2017.06.001

Wang, J. Q., Wan, C. R., Zhou, M., Wang, Z. L., & Yang, M. Z. (2024a). *Investigations on cavitation suppression of bionic water-jet impeller*. Journal of Physics: Conference Series, 2707(1). https://doi.org/10.1088/1742-6596/2707/1/012147

Wang, L. K., Liang, C., Luo, X. Q., Xie, H., Zhu, G. J., Feng, J. J., & Li, C. H. (2024b). *Numerical investigation of cavitation suppression of centrifugal pump based on the bionic humpback whale blade.* Journal of Physics: Conference Series, 2752(1). https://doi.org/10.1088/1742-6596/2752/1/012126

Wang, L., Luo, X., Feng, J., Lu, J., Zhu, G., & Wang, W. (2023). Method of bionic wavy tip on vortex and cavitation suppression of a hydrofoil in tidal energy. *Ocean Engineering* (Jun.15), 278. https://doi.org/10.1016/j.oceaneng.2023.114499

Wang, Y. Y., Zhao, W. G., Han, H. D., Fan, P. J., Liu, Z. L., & Hu, J. Q. (2022). Effects of the centrifugal pump outlet blade angle on its internal flow field characteristics under cavitation condition. *Journal of Applied Fluid Mechanics*, *16*(2), 389-399. https://doi.org/10.47176/jafm.16.02.1241

Weiguo, Z., & Bao, G. (2021). Investigations on the effects of obstacles on the surfaces of blades of the centrifugal pump to suppress cavitation development. *Modern Physics Letters B*, *35*(20). https://doi.org/10.1142/S0217984921503279

Weiguo, Z., & Zhongliang, Z. (2022). Influence of geometric parameters of tiny blades on the shroud of a centrifugal pump on the cavitation suppression effect. *Frontiers in Energy Research*, *10*. https://doi.org/10.3389/fenrg.2022.865885

Wilcox, D. C. & Alem, D. (1994). Simulation of transition with a two-equation turbulence model. *Aiaa Journal*, *32*(2), 247-255. https://doi.org/10.2514/3.59994

Wilcox, D. C. (2008). Formulation of the k - ω Turbulence Model Revisited. Aiaa Journal，46(11), 2823-2838. https://doi.org/10.2514/1.36541

Yan, S., Jiang, Y., & Hu, M. (2022). Study on the cavitation suppression mechanism of axial piston pump. *International Journal of Aerospace Engineering*. https://doi.org/10.1155/2022/9913739

Yuan, S., He, Y., Yuan, J., Cong, X., & Zhao, B. (2006). (2004). Numerical simulation of three-dimensional incompressible turbulent flow field in centrifugal pump impeller with diverting vane. *Journal of Mechanical Engineering* (11), 153-157. https://link.cnki.net/doi/10.3321/j.issn:0577-6686.2004.11.029

Yun, W., Liang, D., Jianwei, W., Zhijian, L., & Wei, W. (2023). *Simulation study on active cavitation suppression for a typical hydrofoil*. Journal of Physics: Conference Series, *2441*(1). https://doi.org/10.1088/1742-6596/2441/1/012043

Zakir, K., & Zhao, W. (2024). Cavitation mitigation via curvilinear barriers in centrifugal pump. *Discover Mechanical Engineering*, *3*(1). https://doi.org/10.1007/s44245-024-00045-8

Zhu, Y., Zhou, L., Lv, S., Shi, W., Ni, H., Li, X., Tao, C., & Hou, Z. (2024). Research progress on identification and suppression methods for monitoring the cavitation state of centrifugal pumps. *Water*, *16*(1), 52. https://doi.org/10.3390/w16010052

Zwart, P. J., Gerber, A. G., & Belamri, T. (2004). *A two-phase flow model for predicting cavitation dynamics*. Proceedings of the Fifth International Conference on Multiphase Flow, Yokohama, Japan, 152, 11.